DRAFT VERSION NOVEMBER 22, 2021
Typeset using LaTeX **twocolumn** style in AASTeX62

arXiv:1912.02701v1 [astro-ph.EP] 5 Dec 2019

Superabundance of Exoplanet Sub-Neptunes Explained by Fugacity Crisis

EDWIN S. KITE,[1] BRUCE FEGLEY JR.,[2] LAURA SCHAEFER,[3] AND ERIC B. FORD[4,5,6,7]

[1]*Department of the Geophysical Sciences, University of Chicago, Chicago, IL (kite@uchicago.edu).*
[2]*Planetary Chemistry Laboratory, McDonnell Center for the Space Sciences & Department of Earth & Planetary Sciences, Washington University, St Louis, MO .*
[3]*School of Earth Sciences, Stanford University, Palo Alto, CA.*
[4]*Department of Astronomy and Astrophysics, The Pennsylvania State University, University Park, PA*
[5]*Center for Exoplanets and Habitable Worlds, The Pennsylvania State University, University Park, PA*
[6]*Institute for CyberScience*
[7]*Pennsylvania State Astrobiology Research Center*

ABSTRACT

Transiting planets with radii 2-3 $R_\oplus$ are much more numerous than larger planets. We propose that this drop-off is so abrupt because at $R \sim 3$ $R_\oplus$, base-of-atmosphere pressure is high enough for the atmosphere to readily dissolve into magma, and this sequestration acts as a strong brake on further growth. The viability of this idea is demonstrated using a simple model. Our results support extensive magma-atmosphere equilibration on sub-Neptunes, with numerous implications for sub-Neptune formation and atmospheric chemistry.

Keywords: Extrasolar rocky planets — Exoplanet atmospheres — Exoplanets: individual (π Mensae c, GJ 3470b, HD 97658b, GJ 9827d, TOI 270 c, GJ 143 b, GJ 436 b, GJ 1214 b, GJ 3470 b, GJ 9827 d, GJ 1132 b, HAT-P-11 b, HAT-P-26 b, HD 3167, HD 15337, HD 21749 b, HD 97658 b, HD 213885 b, HD 219134, HIP 116454b, HR 858, Kepler 10c, Kepler-11, Kepler-21, Kepler-22, Kepler-36c, Kepler-37d, K2-3, K2-18b, K2-21, K2-25, K2-36c, Kojima-1Lb, L 98-59 d, LHS 1140 b, LTT 9779b, 55 Cnc e, π Mensae c, TOI-270, TOI-402.02, WASP-47d, WASP-107b, Wolf 503 b).

1. INTRODUCTION.

According to *Kepler* data, the intrinsic frequency of 2.7-3.0 $R_\oplus$ planets is (4-10)$\times$ that of planets that are only 20% bigger (3.3-3.7 $R_\oplus$) (for $p < 100$ d; Fulton and Petigura 2018; Hsu et al. 2019). This drop-off, or cliff, is the most dramatic feature in the planet-radius histogram (Fig. 1). The radius cliff separates sub-Neptunes, which are intrinsically common, from intrinsically rare Neptune-sized and larger planets. What censors planet growth beyond $\sim$3 $R_\oplus$? Here we propose a new explanation for the steepness (amplitude) and location of the radius cliff. We attribute both to increased solubility of hydrogen in magma at pressures $>10^9$ Pa. We assign this consequence of non-linear hydrogen solubility for sub-Neptune radii a short-hand name, the *fugacity crisis*.

The *Kepler* sub-Neptunes are made of Earth-composition cores (silicates, plus Fe-metal) shrouded by hydrogen-dominated atmospheres, based on strong (though indirect) arguments (e.g., Rogers et al. 2011; Owen & Wu 2017; Van Eylen et al. 2018; Jin and Mordasini 2018; Carrera et al. 2018). We will accept (for the purposes of this paper) those arguments, which imply that *Kepler* sub-Neptunes are mostly core by mass, and mostly atmosphere by volume. Because the cores only rarely exceed $\sim$20% of sub-Neptune volume, the cliff must correspond to a cut-off in atmosphere volumes. Atmosphere volume is a proxy for atmosphere mass M_{atm}(Lopez & Fortney 2014), so the cliff signifies an upper limit on M_{atm} of O(2 wt%) of core mass (M_{core}). This is much less than the O(100 wt%) associated with runaway growth into a gas giant (Pollack et al. 1996). As a result, the upper limit on atmosphere masses cannot be simply explained by core accretion runaway.

Previous attempts to explain the radius cliff have considered both H_2 accretion and H_2 loss. For a given planet mass, large atmospheres are more weakly bound, and lost more readily (e.g. Owen & Wu 2017). However, it is unclear if the steepness of the cliff can be explained by H_2 loss given the wide range of measured sub-Neptune masses (e.g., Rice et al. 2019). In an alternative model by Lee and Chiang (2016), the role of atmosphere accretion is emphasized. In this model, cores – which are treated as chemically and thermally inert – receive an atmosphere transfusion from protoplanetary disks just as those disks expire; because gas is sparse during this brief epoch, the atmosphere dose is O(2 wt%). This model may help to explain the scarcity of $p < 100$ d gas giants and matches pre-2018 data. However it is dependent on disk/nebula-era transients, and because disks vary in their properties and lifetimes, it is difficult to see how it can be solely responsible for the steepness of the cliff (Fig. 1). Moreover, the assumption of chemically and thermally inert magma is questionable (e.g., Ginzburg et al. 2018; Vazan et al. 2018). Hence we seek an alternative explanation.

We are prompted to seek such an explanation in the material properties of H_2, specifically the solubility of H_2 in magma. The pressure at the atmosphere-core boundary on sub-Neptunes is $P_{atm} \approx M_{atm}\overline{g}/A_{pl}$, where $\overline{g}$ is the magnitude of gravitational acceleration in the atmosphere (using a mass-weighted average), and $M_{atm} \ll M_{core}$. So, if $\overline{g} = \epsilon G M_{core}/R_{core}^2$ (where R_{core} is core radius), then $P_{atm} \approx \epsilon M_{atm}(GM_\oplus/4\pi R_\oplus^4)$, where $\epsilon < 1$ is a correction for lower gravity higher in the atmosphere. Here we set $R_{core}/R_\oplus \sim (M_{core}/M_\oplus)^{1/4}$ (cores are modestly compressible; Valencia et al. 2006). This yields

$$P_{atm} \approx 5 \times 10^9 \,\mathrm{Pa}\, \epsilon \left(\frac{f_{atm}}{0.01}\right)\left(\frac{M_{core}}{4M_\oplus}\right) \quad (1)$$

where $f_{atm} = M_{atm}/M_{core}$. Such deep atmospheres slow the cooling of initially molten planetary cores, so most transiting sub-Neptunes will still have a magma ocean in contact with the atmosphere, defining a *magma-atmosphere interface* at which solubility equilibrium should hold. For H_2 solubility, 5 GPa is an interesting number. Above 1 GPa, intermolecular repulsion renders molecular H_2 much less compressible (Saumon et al. 1995). (Non-ideal behavior kicks in at much lower pressure than the transition to metallic hydrogen, which occurs at $\gtrsim$100 GPa within planets). The reduced compressibility of molecular H_2 greatly increases the tendency of H_2 to dissolve into adjacent liquid – this tendency is termed fugacity (f, units Pa). To understand this, consider the equation for Gibbs free energy G, dG = PdV - TdS. If we assume isothermal conditions and if ΔV = $V_{(\mathrm{H2,\,in\,melt})}$ - $V_{(\mathrm{H2,gas})}$ is negative, then ΔG favors dissolution. For example, at (1.5-3) GPa, the density of H_2 gas is 40-80 kg/m^3, much less than the 180 kg/m^3 partial density of H_2 in basaltic melt (Hirschmann et al. 2012). As long as the dissolved H_2 compressibility exceeds that of the gas at higher P, dissolution remains favored. Even for the $f = p$ limit, which is appropriate for <1 GPa, the H content of the magma can exceed the H content of the atmosphere (Chachan & Stevenson 2018). Above 1 GPa, $f_{\mathrm{H2}} \gg P_{\mathrm{H2}}$ (Fig. 2a). This suggests that the ramp-up in dissolution of the atmosphere into magma for $P_{atm} > 1$ GPa might lead to greater and greater partitioning of added nebula gas into the magma as planet radius (and thus atmospheric mass) increases. We term this a *fugacity crisis* (Fig. 2b).

2. METHOD.

We seek to explain the 3 $R_\oplus$ cliff, not the divot ("radius valley") at ~2 $R_\oplus$. Previous studies have proposed explanations for the radius valley, including gas escape-to-space (e.g. Owen & Wu 2017; Ginzburg et al. 2018; Gupta, & Schlichting 2019). We neglect gas escape-to-space, and our model is not intended to match the radius valley.

To see if the fugacity crisis can generate a radius cliff, our minimal model includes:

(a) H_2 solubility as a function of P_{atm} and the temperature at the magma-atmosphere interface (T_{mai}) (Fig. 2a);

(b) P_{atm} as a function of atmosphere mass;

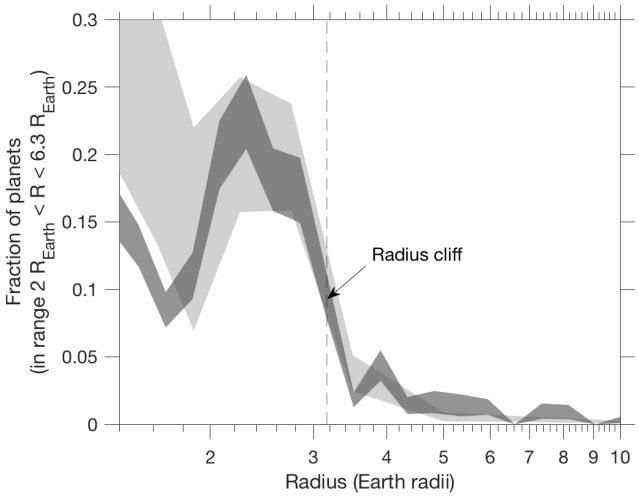


Figure 1. The exoplanet radius distribution, according to Fulton and Petigura (2018) (dark gray band, $\pm1\sigma$), and according to Hsu et al. (2019), (for $p < 64$ days, light gray band, $\pm1\sigma$). Hsu et al. (2019) data are adjusted downward by a factor of 2.25 in order to compensate for different bin choices. The dashed line at 3.16 $R_\oplus$ highlights the radius cliff.

(c) An expression for the mass of magma as a function of planet mass, tracking magma crystallisation at low T_{mai}.

Details of (a)-(c) are provided below. By combining (a)-(c), we can calculate the partitioning of H_2 between the magma and the atmosphere (Fig. 2b).

(a) Getting H solubility as a function of pressure and temperature requires fugacity coefficients, an experimental fugacity↔solubility calibration, and a temperature dependence parameterization (Kite et al. in review.). The fugacity coefficient of H_2, ϕ, is computed using

$$\ln\phi = \ln\frac{f}{P} = \int_0^P \left(\frac{Z-1}{P}\right) dP \quad (2)$$

where the compressibility factor Z is given by $Z = (PV_m)/(RT)$. Here, V_m is the molar volume, obtained from the Saumon et al. (1995) tables assuming pure molecular H_2 (we set Z = 1 below 10^7 Pa to minimize the effect of thermal dissociation). When ϕ = 1, the gas behaves ideally. ϕ >10 by 8 GPa (Fig. 2a). The H_2 solubility at the magma-atmosphere interface is set to

$$X_{\mathrm{H2}} = 1 \times 10^{-11}\, f_{\mathrm{H2}} \exp(-T_0/T_{mai}) \quad (3)$$

where X_{H2} is the mass fraction. (X_{H2} is not permitted to exceed 50 wt%.) This follows the estimated molten-average-rock solubility from Hirschmann et al. (2012) (i.e., the estimated peridotite solubility). This solubility is ~5× lower than was used by Chachan & Stevenson (2018). T_0 is uncertain; we use 4000 K (following Chachan & Stevenson 2018). There are no direct measurements of H_2 solubility in magma at ~3000 K.

(b) To relate f_{atm} to P_{atm}, for $P_{atm} < 100$ bars we assume $\overline{g} = GM_{core}/R_{core}^2$. For thicker atmospheres, we use

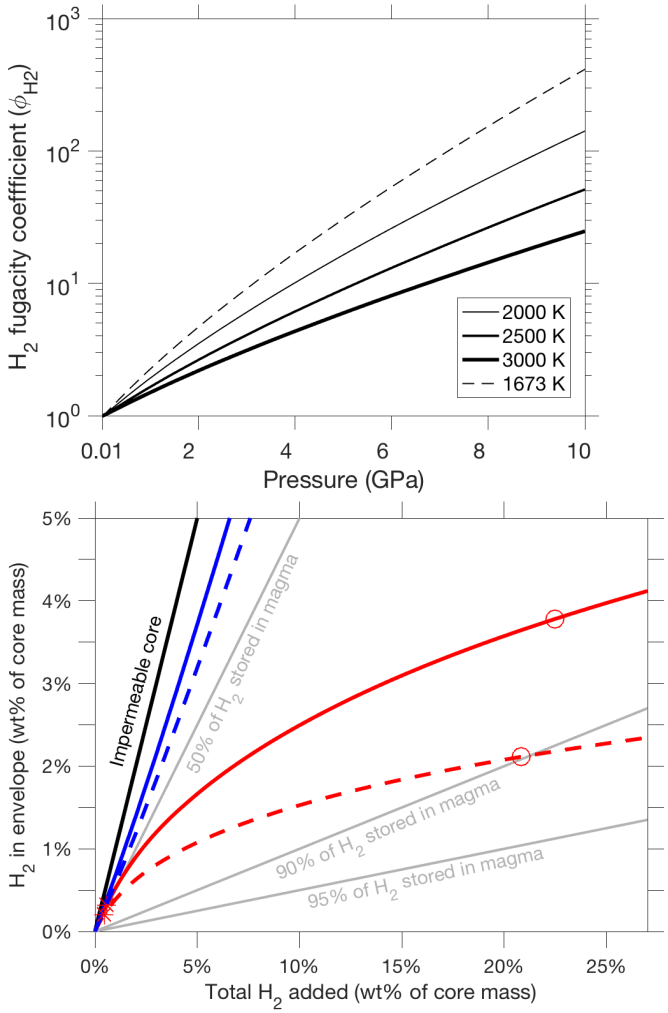


Figure 2. (a) Fugacity coefficients for H_2. (b) The fugacity crisis for magma-atmosphere interface temperature (T_{mai}) = 3000K. The 1:1 line is the inert impermeable core assumption ("all-H_2-in-atmosphere"), used in all but one previous study. The thick blue lines are for the ideal (Henry's Law) dissolution case. The red lines include nonideal dissolution of H_2 into magma. Red asterisks show P_{atm} = 1 GPa and red open circles show P_{atm} = 8 GPa. The solid lines show M_{core} = 4 $M_\oplus$. The dashed lines show M_{core} = 8 $M_\oplus$.

the hydrogen equation-of-state of Saumon et al. (1995) to construct adiabatic density-height (ρ-z) profiles up from the bottom-of-atmosphere temperature (assumed equal to T_{mai}) in order to obtain $\overline{g}$. We multiply densities by 120% to account for non-H_2 species. This approach is intended only to make a first-order correction for the reduced gravity within the atmosphere, and we do not use the output to get the planet transit radius. We also ignore the top-of-atmosphere T from this workflow (typically 500-1500 K at 100 bars). Instead, we treat T_{mai} as a free parameter (sub-Neptune core cooling calculations output T_{mai} = 3000±1500 K; e.g., Howe & Burrows 2015; Vazan et al. 2018; Bodenheimer et al. 2018).

(c) Molten rock can store very much more volatiles than solid rock. To obtain the mass of rock that is molten and so can store H_2, we follow Kite et al. (in review.). Within a convecting magma ocean, $\partial T_{melt}/\partial z > \partial T_{adiabat}/\partial z$ for $P < 10^2$ GPa. Here, T_{melt} is the temperature corresponding to 40 wt% melt fraction, and $T_{adiabat}$ is the temperature within the convecting magma. Thus, sub-Neptunes plausibly have magma shells overlying solid silicates. To find magma shell thickness, we interpolate and extrapolate the solidus (0% melting curve), the liquidus (100% melting curve), and the magma adiabats of Figure 5 from Andrault et al. (2011). We integrate down from the magma-atmosphere interface until the adiabat reaches the solidus. To do this, we extrapolate the silicate density as a function of pressure from Dziewonski & Anderson (1981). The T_{mai} = 3000 K adiabat is hotter than the solidus for chondritic-primitive-mantle material for $P < 130$ GPa according to Andrault et al. (2011). We make the approximation that at $T_{mai} \geq 3000$ K, sub-Neptune silicates are fully molten. We assume that silicates make up 2/3 of the mass of the planet core. This very basic model is sufficient for our purposes; see (e.g.) Bower et al. (2019) and Dorn et al. (2017) for more sophisticated models.

We compute planet radii based on f_{atm}, using the planet transit radius look-up tables of Lopez & Fortney (2014), for solar-composition opacity and planet age ≥1 Gyr.

So far, we described calculations for one planet, but our goal is to compare to the planet radius histogram. In order to generate synthetic planet histograms, we need a prior distribution on the variability of the total amount of H_2 supplied by the nebula to the core. As shown in Fig. 4, the existence and approximate location of the cliff has low sensitivity to reasonable variations for the choice of prior.

3. RESULTS.

3.1. *The Crisis in H_2 Partitioning*

The crisis in H_2 partitioning is shown in Fig. 2b. For <0.5 wt% of H_2 added, for T_{mai} = 3000 K and a 5 $M_\oplus$ core, most of the H_2 stays in the atmosphere. However, as the total H_2 added is increased, it becomes very difficult to increase the mass of H_2 in the atmosphere because solubility increases exponentially with P_{atm} (Fig. 2a). This is the fugacity crisis. For 10 $M_\oplus$ cores, exceeding 1.5 wt% H_2 in the atmosphere requires >20% H_2 to be added, and beyond this point almost all of each additional parcel of H added goes into the core.

3.2. *The Fugacity Crisis Can Explain the Radius Cliff At 3 $R_\oplus$*

Fig. 3 shows the reference results. With a smooth distribution of gas supply, both the impermeable-core case (black line) and the linear-solubility, Henry's Law case (blue line) yield a broad distribution for radii. Neither model predicts a cliff.

However, the observed radius cliff is reproduced by the fugacity crisis model. Below ∼2.2 $R_\oplus$ (corresponding to 1 GPa), non-ideal effects are small, and the red line closely tracks the blue line. Between 1 GPa and 8 GPa (radius 2.2-3.6 $R_\oplus$) the non-ideal effects are so strong as to define a sharp

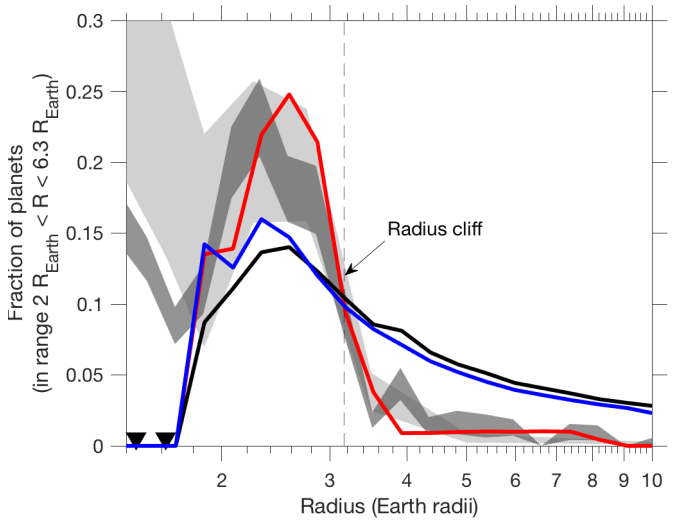


Figure 3. Histograms of planet abundance. Colored bands are the true planet histogram ($\pm 1\sigma$ error) according to Hsu et al. (2019) (light gray) and according to Fulton and Petigura (2018) (dark gray). Lines show model output for the impermeable planet case (black line); linear (Henry's Law) dissolution (blue line); and the fugacity-crisis case (red line). Parameters: M_{core} drawn with equal likelihood from {4,5,6} $M_\oplus$, T_{mai} = 3000 K, solar-composition atmospheric opacities, insolation 1000 $L_\oplus$, planet age 1 Gyr, and a log-gaussian distribution of gas supply centered on 5 wt% of core mass, with a standard deviation of 1 dex in gas supply, and an upper limit of 50 wt% (above this limit, we implicitly assume, gravitational runaway will cause planets to explode into exo-Jupiters.) Model output bins are the same as in Fulton et al. (2017).Triangles correspond to the bare-core radii for 4 and 6 $M_\oplus$.

concentration and a sharp fall-off in planet radii. Essentially, transiting planets with radii 2-3 $R_\oplus$ are so numerous because at $R \sim 3$ $R_\oplus$, base-of-atmosphere pressure becomes large enough for the atmosphere to readily dissolve into magma. This sequestration greatly slows the rate of growth in planet radius, even as the planet continues to accrete gas.

All three models shown in Fig. 3 underpredict the inferred planet occurrence rate for planets smaller than $\sim$1.8 $R_\oplus$ due to the limitations of our model which focuses on the interaction of gas and silicates. Creating smaller planets would require planet core masses less than 4 $R_\oplus$, the smallest core mass in our simulations. Accurately modeling the occurrence rate of smaller planets would require a model for the distribution of core masses and compositions. Similarly, the predictions for radii larger than $\sim$5 $R_\oplus$ are not realistic, since our model does not include runaway accretion of gas once the atmosphere mass dominates the core mass. Runaway accretion will further depopulate the 3-6 $R_\oplus$ region of the plot, so runaway will result in a further decrease in the rate of these planets.

Fig. 4 shows the results of several variations on our reference model that serve as tests of the sensitivity of the fugacity crisis to model parameters. Fig. 4a shows that raising core mass from 4 $M_\oplus$ to 8 $M_\oplus$ shifts the cliff location by $\sim$0.4 Earth radii. For smaller core masses the weight per unit mass of the atmosphere is less, so more H_2 mass can be added before reaching the limiting P_{atm}.

Fig. 4b shows that decreasing insolation from 1000 $L_\oplus$ to 10 $L_\oplus$ shrinks the planets by 0.25 $R_\oplus$ (dashed lines). The effect of increasing planet age from 1 Gyr to 10 Gyr (dash-dot line) is similar. Reducing H_2 solubility by a factor of 10 moves the cliff to larger radius by $\sim$0.7 $R_\oplus$ (dashed line).

Fig 4c shows results for T_{mai} = 2500 K. The melt mass is greatly reduced (and insensitive to planet mass; 0.5-0.7 $M_\oplus$ of melt for M_{core} = 1-10 $M_\oplus$). This effect overpowers the greater solubility of H_2 in magma at lower T (Fig. 2a). Because there is less melt into which H_2 can dissolve, the amplitude of the cliff is reduced. However the results for incomplete melting are sensitive to the value of the maximum H_2 content of magma, which is poorly constrained.

Fig 4d shows the results for a log-uniform distribution of gas supply between bounds of 0.1 wt% and 30 wt% of core mass. The basic pattern is independent of choice of prior: the cliff gets steeper for non-ideal fugacity, and is especially steep for larger (8 $M_\oplus$) core masses.

As shown in Fig. 4, the precise location and amplitude of the fugacity cliff depends on model parameters, including the distribution of core masses, atmosphere mass fractions, insolations, and T_{mai}. Nevertheless, these results show that a fugacity crisis is robust and can explain both the amplitude and the position of the radius cliff.

4. DISCUSSION.

4.1. *Approximations and Limitations*

Our model provides a simple, equilibrium explanation for the radius cliff. However, this simplified model has limitations.

The most important limitation is the lack of H_2 solubility-in-magma data in the $\sim$4000 K and $10^9 - 10^{10}$ Pa regime of the sub-Neptune magma-atmosphere interface. This lack is understandable, because under such conditions magma is literally uncontainable (in that all material containers will melt). Nevertheless, more laboratory and/or numerical experiments are motivated. Meanwhile, we extrapolate from lower-temperature, lower-pressure data (Hirschmann et al. 2012).

Another approximation is that we do not explicitly model partial molar volume of the dissolved gas. Including this effect would decrease solubilities and increase core volume, boosting planet radii. The addition of dissolved gas to the magma will also increase gravity throughout the atmosphere, which (because solubility depends on P_{atm}) shrinks radii. Determining which of these effects dominates would require a more sophisticated interior model.

Alternative choices for silicate composition could give a solidus and liquidus hotter by up to 1000 K, curtailing melting (Andrault et al. 2017). On the other hand, real sub-Neptune T_{mai} could be >4000 K, according to thermal models (e.g. Howe & Burrows 2015; Bodenheimer et al. 2018). Moreover, volatile addition favors melting; an effect we omit. Therefore, it is not clear whether or not our simple procedure

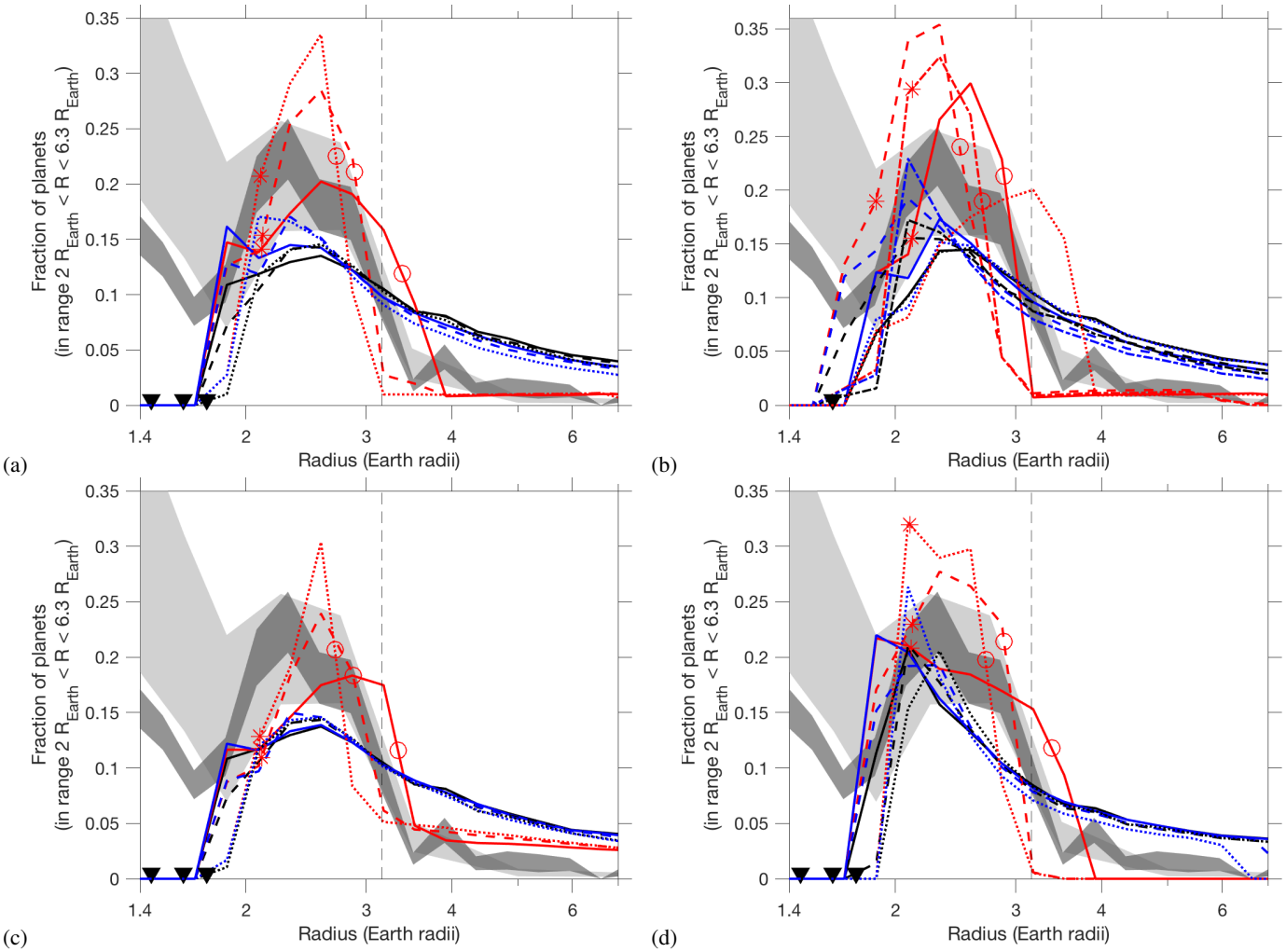


Figure 4. Histograms of planet abundance showing sensitivity to parameters. In each panel, the colored bands are the true planet histogram ($\pm 1\sigma$ error) according to Hsu et al. (2019) (light gray) and according to Fulton and Petigura (2018) (dark gray). The black lines show the impermeable-planet cases. The blue lines show the linear (Henry's Law) dissolution cases. The red lines show the fugacity-crisis cases. For the red lines, the asterisks show atmosphere-base pressure = 1 GPa and the open circles show P_{atm} = 8 GPa. Model output bins are the same as in Fulton et al. (2017), and the triangles correspond to the bare-core radii for the specified masses. (a) Sensitivity to core mass. Solid, dashed, and dotted lines are for 4 $M_\oplus$, 6 $M_\oplus$, and 8 $M_\oplus$ respectively. This reference case shows model output for 1 Gyr, solar metallicity, T_{mai} = 3000 K, insolation 1000 $L_\oplus$. (b) Solid lines show the 6 $M_\oplus$ case from panel a. The dashed lines vary L, which is set to 10 $L_\oplus$. The atmosphere is colder, but the magma is held at 3000 K. The dash-dot lines vary planet age, which is set to 10 Gyr. The dotted lines decrease the H_2 solubility by a factor of 10. (c) As panel a, but for T_{mai} = 2500 K. (d) As panel a, but a log-uniform prior between bounds of 0.1 wt% and 30 wt% H_2 added.

overstates or understates magma mass. If the fugacity crisis hypothesis passes the tests we propose (§4.2), then the need for some melt in order to sequester H could provide a joint constraint on the temperature and silicate composition of cores.

As more atmosphere dissolves in the melt and vice versa, distinctions between melt and atmosphere must vanish. For example, reactions exemplified by $4H_2$ + $SiO_{2(\mathrm{melt})}$ = $SiH_{4(gas)}$ + $2H_2O_{(\mathrm{gas})}$ can lead to partial dissolution of the cores in the atmosphere. This is potentially testable by observations of SiH_4 and other hydride/hydroxide gases of the rock forming elements. As the conditions for full magma-atmosphere miscibility emerge during planet formation, a fuzzy zone will develop at the magma-atmosphere interface. This zone is buoyant relative to the volatile-poor earlier-formed core. It is not known if convective transport through fuzzy zones is totally shut down, or merely reduced (Garaud 2018). In either case, fuzzy-zone development at the atmosphere-core interface would restrict further dissolution of the atmosphere into the magma.

Our model ignores H_2O, so it does not apply to Neptune and Uranus, which are probably (although not certainly) H_2O-rich (Helled et al. 2019).

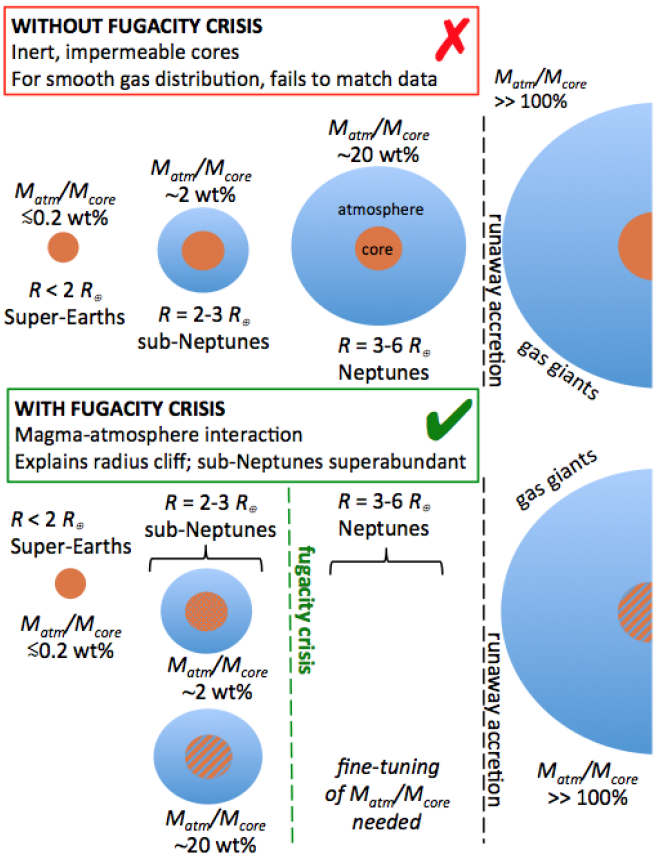


Figure 5. Graphical abstract of this paper.

Although we assume the total amount of H_2 supplied by the nebula to the core is commonly in the range 0.1-100% of core mass, our model says nothing about why this should be. Thus, our model complements studies of gas supply from the nebula to the core (e.g., Lee and Chiang 2016).

4.2. *Alternatives and Tests*

If the magma ocean and the atmosphere equilibrate, then escape-to-space models understate the amount of gas that must be removed to affect planet radii. This is because gas loss will be compensated by exsolution – a negative feedback (Fig. 2b). This increases the energy demand on escape-to-space models. Moreover, if H_2 dissolves into magma then the planet's radius will be smaller during the crucial first 100 Myr, when the XUV flux is greatest. In effect, the atmosphere hunkers down, reducing the number of hits from the XUV-photon fusillade. Moreover, the dissolved-in-magma H_2 will not be directly ejected by giant-impact shocks. These considerations suggest that *if* the magma ocean and the atmosphere equilibrate, then the fugacity crisis is the only explanation for the cliff.

The hypothesis of magma-atmosphere equilibration makes the following testable predictions.

1. *Cliff Steepness.* The fugacity crisis hypothesis is motivated by cliff steepness (Fig. 1). If more data and analysis makes this cliff less steep, that would not disprove the fugacity crisis, but it would dilute the attractiveness of this physics playing a dominant role in shaping final planet radii.
2. *Insensitivity To Formation Environment, Host Star Mass, e.tc.*. As an equilibrium explanation, the fugacity crisis applies regardless of disk lifetime, host star mass, etc. Therefore, this model would be disfavored by a strong dependence of cliff location on star mass (for example).
3. *Atmospheric Chemistry*. The fugacity crisis model requires a large amount of magma to interact with the atmosphere. Due to differential solubility (and likely partitioning of C into the Fe-metal-phase; Dasgupta & Grawal 2019), this will drive elemental ratios (e.g. C/O) away from the solar value. This can now be tested (e.g. Benneke et al. 2019).
4. *Mass Dependence of Cliff Position.* Our model predicts that more-massive planets (as a set) should have a cliff position that is at smaller radius than less-massive planets (as a set). This assumes that f_{atm} is independent of core mass. This prediction is in tension with the radius analysis of Wu (2019). This motivates precision radial velocity surveys of a large number of planetary systems, ideally with multiple transiting planets.
5. *Gentler Slope For Longer Periods and Older Stars*. The ensemble of sub-Neptunes with magma-atmosphere interfaces that are cold enough to crystallize (longer periods and older stars) should have a gentler cliff slope and thus a greater proportion of $\gtrsim 4$ $R_\oplus$ planets. This is because core crystallization reduces the extent to which the magma can store hydrogen. This motivates future transit surveys that significantly increase the number of stars surveyed for transiting planets with equilibrium temperatures less than 400 K.

4.3. *What Do Active Cores Imply?*

The growth process and the birth location for sub-Neptunes are unknown (e.g., Rogers et al. 2011; Chiang and Laughlin 2013; Chatterjee and Tan 2014; Levison et al. 2015; Ormel 2017; Mordasini 2018; Brouwers et al. 2018).

Our model assumes chemically (and thus thermally) active cores, with magma-atmosphere equilibration. Equilibration will happen if the silicates are delivered as planetesimals or as pebbles after the atmosphere has formed (Bodenheimer et al. 2018). If the silicates and gas are accreted on similar timescales, then interaction would occur at progressively higher pressures during planet formation. Our model is an equilibrium explanation which assumes that during or after planet growth this history of planet assembly is stirred away. Stirring need not be complete in order for the fugacity crisis to explain the radius cliff, because a little bit of magma can make a big difference (Fig. 4c).

Pursuit of these tests and implications will be aided by future extended missions for TESS (Huang et al. 2018); PLATO; ARIEL; and more radial-velocity data for sub-Neptunes.

5. CONCLUSION.

The major feature in the exoplanet radius distribution is the rapid decrease in the occurrence rate of planets as size increases from 3 to 3.5 $R_\oplus$. This can be understood as a consequence of the nonideal increase in H_2 fugacity above 1 GPa. As the base-of-atmosphere pressure approaches 10 GPa ($\sim 3R_\oplus$), more and more of the added H_2 goes into the magma and so the radius does not increase much.

It follows that H_2 supply from the nebula can have a broad mass distribution and still match the observed radius histogram. A world with <1 wt% H_2 can lose its atmosphere and become a Super-Earth; a world with a few wt% H_2 becomes a sub-Neptune; a world with $\sim$20 wt% H_2 *also* becomes a sub-Neptune because of the fugacity crisis described above; and a world with a ratio of H_2 mass to core mass of $O(100\%)$ undergoes gravitational runaway and becomes a gas giant (Fig. 5). The main strength of the fugacity crisis hypothesis is that it is an equilibrium explanation; it is less dependent on transients from formation-era processes, which are hard to constrain and thus test. The main weakness of our explanation is that it depends on a limited number of laboratory measurements of H_2 solubility. Better material properties data, including lab and numerical experiments relevant to solubilities under sub-Neptune conditions, are needed to build better models of sub-Neptune evolution (e.g., Hirschmann et al. 2012; Soubiran and Militzer 2015).

The fugacity crisis defines the radius cliff and so explains why sub-Neptunes are so common while Neptune-sized planets are rare. Although our simple model suggests a solution to one of the puzzles posed by sub-Neptunes, overall, it is striking that the most common type of transiting planet remains so poorly understood.

Acknowledgements. We thank M.M. Hirschmann, L.A. Rogers, D. Hsu, and B. Fulton. Grants: NASA (NNX17AC02G, NNX16AB44G), NSF (AST-1517541). E.B.F. acknowledges support from the Center for Exoplanets and Habitable Worlds, which is supported by The Pennsylvania State University, the Eberly College of Science, and the Pennsylvania Space Grant Consortium.

Code availability. Everything used to make this paper can be obtained for unrestricted further use by emailing the lead author.

REFERENCES

Andrault, D., Bolfan-Casanova, N., Nigro, G. L., et al. 2011, E&PSL, 304, 251
Andrault, D., Bolfan-Casanova, N., Bouhifd, M. A., et al. 2017, Phys. Earth & Planet Interiors, 265, 67
Benneke, B., Knutson, H. A., Lothringer, J., et al. 2019, Nature Astronomy, 3, 813
Bodenheimer, P., Stevenson, D. J., Lissauer, J. J., & D'Angelo, G. 2018, ApJ, 868, 138
Bower, D. J., Kitzmann, D., Wolf, A. S., et al. 2019, arXiv:1904.08300
Brouwers, M. G., Vazan, A., Ormel, C. W. 2018. A&A611, A65.
Carrera, D., Ford, E. B., Izidoro, A., Jontof-Hutter, D., Raymond, S. N., Wolfgang, A. 2018. ApJ, 866, 104.
Chachan, Y., & Stevenson, D. J. 2018, ApJ, 854, 21
Chatterjee, S., Tan, J. C. 2014. ApJ 780, 53.
Chiang, E., Laughlin, G. 2013. MNRAS 431, 3444-3455.
Dasgupta, R. & D.S. Grawal 2019, Origin and early differentiation of carbon and associated life-essential volatile elements on Earth, *in* Deep Carbon: Past to Present, Cambridge University Press.
Dorn, C., Venturini, J., Khan, A., et al. 2017, A&A, 597, A37
Dziewonski, A. M., & Anderson, D. L. 1981, Physics of the Earth and Planetary Interiors, 25, 297
Fulton, B. J., Petigura, E. A., Howard, A. W., et al. 2017, AJ, 154, 109
Fulton, B. J., Petigura, E. A. 2018. AJ, 156, 264.
Garaud, P. 2018, Annual Review of Fluid Mechanics, 50, 275
Ginzburg, S., Schlichting, H. E., Sari, R. 2018. MNRAS 476, 759-765.
Gupta, A., & Schlichting, H. E. 2019, MNRAS, 487, 24
Helled, R., Nettelmann, N., & Guillot, T. 2019, arXiv:1909.04891
Hirschmann, M. M., Withers, A. C., Ardia, P., & Foley, N. T. 2012, E&PSL, 345, 38
Howe, A. R., & Burrows, A. 2015, ApJ, 808, 150
Hsu, D. C., Ford, E. B., Ragozzine, D., & Ashby, K. 2019, arXiv:1902.01417
Huang, C. X., Shporer, A., Dragomir, D., et al. 2018, arXiv:1807.11129
Inamdar, N. K., Schlichting, H. E. 2016. ApJ 817, L13.
Jin, S., Mordasini, C. 2018. ApJ, 853, 163.
Kite, E. S., Fegley, B., Schaefer, L., & Ford, E. B., in review.
Lee, E. J., Chiang, E. 2016. ApJ 817, 90.
Levison, H. F., Kretke, K. A., Walsh, K. J., Bottke, W. F. 2015. PNAS 112, 14180-14185.
Lopez, E. D., & Fortney, J. J. 2014, ApJ, 792, 1.
Mordasini, C. 2018. Handbook of Exoplanets, id. 143.
Ormel, C. W. 2017. Astrophysics and Space Science Library 445, 197.
Owen, J. E., & Wu, Y. 2017, ApJ, 847, 29
Pollack, J. B., Hubickyj, O., Bodenheimer, P., et al. 1996, Icarus, 124, 62
Rice, K., Malavolta, L., Mayo, A., et al. 2019, MNRAS, 484, 3731
Rogers, L. A., Bodenheimer, P., Lissauer, J. J., Seager, S. 2011, ApJ, 738, 59.
Saumon, D., Chabrier, G., van Horn, H. M. 1995. ApJS, 99, 713.
Soubiran, F., Militzer, B. 2015. ApJ 806, 228.
Valencia, D., O'Connell, R. J., & Sasselov, D. 2006, Icarus, 181, 545
Van Eylen, V., Agentoft, C., Lundkvist, M. S., et al. 2018, MNRAS, 479, 4786
Vazan, A., Ormel, C. W., Noack, L., Dominik, C. 2018. ApJ 869, 163.
Wu, Y. 2019. ApJ, 874, 91.